EPJ Web of Conferences **3**, 06009 (2010)
DOI:10.1051/epjconf/20100306009

Three-body Faddeev like approach to direct nuclear reactions

A.C. Fonseca[1,a] and A. Deltuva[1]

Centro de Física Nuclear da Universidade de Lisboa, P-1649-003 Lisboa, Portugal

Abstract. Momentum space three-body Faddeev-like equations are used to calculate elastic, transfer and charge exchange reactions resulting from the scattering of deuterons on ^{12}C and ^{16}O or protons on ^{11}Be, ^{13}C and ^{17}O; ^{10}Be, ^{12}C and ^{16}O are treated as inert cores. All possible reactions are calculated in the framework of the same model space. Comparison with previous calculations based on approximate methods used in nuclear reaction theory is discussed.

1 Introduction

As discussed in the review article by Austern *et al.* [1] twenty years ago, three-body models of deuteron-induced reactions became important since the early studies of stripping theory [2], where "the internal coordinates of the target nucleus are ignored and the only dynamically active variables are the coordinates, relative to the target nucleus, of the interacting nucleon that is captured by the nucleus and the spectator nucleon that goes on to the detector".

The present work goes back in time, recaptures the three-body concept of direct nuclear reactions that is common to continuum discretized coupled channels (CDCC) calculations [1] and shows the results obtained by solving Faddeev/Alt, Grassberger, and Sandhas (AGS) equations [3–5] for elastic, transfer and breakup reactions where three-body dynamics plays a dominant role. In this work we attempt to calculate all observables using dynamical models based on energy-independent or energy-dependent optical potentials for the nucleon-nucleus interaction [6] and realistic neutron-proton (np) potentials such as CD-Bonn [7]. Some examples are shown for reactions initiated by deuterons on ^{10}Be, ^{12}C and ^{16}O, as well as protons on ^{11}Be, ^{13}C and ^{17}O. Although the use of energy-dependent potentials in three-body calculations is not free of theoretical problems that are discussed below, the results we show demonstrate the possibilities and the shortcomings of this model; this is, above all, the aim of the present paper.

Although deuteron-nucleus three-body models, including striping or pick up, have already been explored in the past in the framework of Faddeev/AGS equations starting with the pioneer work of Aaron and Shanley [8] to the more recent calculations of Alt *et al.* [9], all of them were drastically simplified. In most cases separable interactions were used between pairs and the correct treatment of the Coulomb interaction was missing. This situation has now changed due to the recent progress in the description of proton-deuteron elastic scattering and breakup [10,11] where the Coulomb repulsion is fully included using the method of screening and renormalization [12,13] together with realistic nuclear potentials. This technical development was applied to three-body nuclear reactions to test the accuracy of the CDCC method [14] and the convergence of the multiple scattering series in the framework of the Glauber approximation [15] and distorted-wave impulse approximation (DWIA) [16] which are standard approximations used to describe nuclear reaction data.

Some of the interaction models employed in this work and in CDCC calculations are formally identical, but instead of solving the three-body Schrödinger equation in coordinate space using a representation in terms of a set of eigenstates pertaining to a given subsystem Hamiltonian, we solve the Faddeev/AGS equations in momentum space and obtain numerically well converged solutions of the three-body problem for all reactions allowed by the chosen interactions. In Ref. [14] we benchmarked the two methods and concluded that CDCC is indeed a reliable method to calculate deuteron-nucleus elastic and breakup cross sections, but may not provide a sufficiently accurate solution of the three-body problem for transfer and breakup in one-neutron halo nucleus scattering from a proton target such as ^{11}Be + p reactions. In those cases the comparison of CDCC results with experimental data may be misleading.

In Sec. 2 we recall the Faddeev/AGS equations, in Sec. 3 we present the results for three dynamical models. Conclusions are given in Sec. 4.

2 The Three-Body Equations

Let's consider a system of three particles ($\alpha = 1, 2, 3$) with kinetic energy operator H_0, interacting by means of two-body potentials v_α ($v_1 = v_{23}$ in the standard odd-man-out notation). The full resolvent

$$G(Z) = (Z - H_0 - \sum_\sigma v_\sigma)^{-1} \qquad (1)$$

[a] e-mail: fonseca@cii.fc.ul.pt

and the channel resolvent

$$G_\alpha(Z) = (Z - H_0 - v_\alpha)^{-1} \quad (2)$$

may be related through the AGS transition operator $U_{\beta\alpha}(Z)$ as

$$G(Z) = \delta_{\alpha\beta}\, G_\alpha(Z) + G_\beta(Z) U_{\beta\alpha}(Z) G_\alpha(Z). \quad (3)$$

The transition operator $U_{\beta\alpha}(Z)$ satisfies the AGS equation [4]

$$U_{\beta\alpha}(Z) = \bar{\delta}_{\beta\alpha}\, G_0^{-1}(Z) + \sum_\sigma \bar{\delta}_{\beta\sigma}\, T_\sigma(Z)\, G_0(Z) U_{\sigma\alpha}(Z), \quad (4)$$

where the summation on σ runs from one to three, $\bar{\delta}_{\beta\alpha} = 1 - \delta_{\beta\alpha}$, $G_0(Z) = (Z - H_0)^{-1}$ is the free resolvent, and $T_\alpha(Z)$ is the two-body transition matrix (t-matrix) that obeys the Lippmann-Schwinger equation for pair α,

$$T_\alpha(Z) = v_\alpha + v_\alpha\, G_0(Z)\, T_\alpha(Z). \quad (5)$$

At a given energy E in the three-body center of mass (c.m.) system the on-shell matrix elements $\langle \psi_\beta | U_{\beta\alpha}(E + i0) | \psi_\alpha \rangle$ calculated between the appropriate channel states yield all the relevant elastic, inelastic and transfer ($\beta, \alpha = 1, 2, 3$) as well as breakup ($\beta = 0$) amplitudes. The channel state $|\psi_\alpha\rangle$ for $\alpha = 1, 2, 3$ is the eigenstate of the corresponding channel Hamiltonian $H_\alpha = H_0 + v_\alpha$ with the energy eigenvalue E made up by the bound state wave function for pair α times a relative plane wave between particle α and pair α. For breakup the final state is a product of two plane waves corresponding to the relative motion of three free particles.

The AGS equations 4 are Faddeev-like equations with compact kernel and therefore suitable for numerical solution; they are consistent with the corresponding Schrödinger equation and therefore provide exact description of the quantum three-body problem. After partial wave decomposition Eq. 4 becomes a two variable integral equation which we solve by standard discretization of momentum variables and summation of the multiple scattering series by Padé method; more details can be found in Refs. [17,18]. As in all numerical calculations convergence of results has to be tested vis-à-vis number of included partial waves, mesh points and Padé steps.

To include the Coulomb interaction between two charged particles we use the method of screening and renormalization [12,13,10]. The Coulomb potential is screened, standard scattering theory for short-range potentials is used in the form of Eq. 4 with parametric dependence on the screening radius R, and the renormalization procedure is applied to obtain R-independent results for sufficiently large R, that correspond to the unscreened limit. A complete review on this subject is presented in Ref. [19] together with a number of practical applications.

3 The Dynamical Models

In this section we set the three-body dynamics we apply to study all the reactions initiated by deuterons on ^{10}Be, ^{12}C and ^{16}O as well as protons on ^{11}Be, ^{13}C and ^{17}O where ^{10}Be, ^{12}C and ^{16}O are considered as inert cores.

Although in most nuclear reaction calculations the deuteron wave function is generated through a Gaussian potential fitted to the deuteron binding energy, which is then used to drive the np interaction in all other partial waves, we use the CD-Bonn [7] potential as our realistic interaction for all np partial waves including the deuteron channel.

For the neutron-nucleus (nA) and proton-nucleus (pA) interactions we use the optical potentials of Watson *et al.* [6] which are based on an optical model analysis of nucleon scattering from $1p$-shell nuclei between 10 and 50 MeV; the nucleus A is a structureless core of mass number A. Although core excitation may be treated in the present three-body models, we discard such possibility at this time. Therefore the relevant parameters of this optical model fit are both energy and mass dependent and are fitted to the existing data over the energy and mass range. For specific nuclei and energy, one could perhaps obtain a better fit but, as mentioned in the Introduction, our goal is to explore the possibilities of a three-body model that can simultaneously describe all reactions allowed by the chosen interactions and leave the fine tuning for an improved model study. In all calculations nucleons are considered as spin $1/2$ particles and the nuclear cores as spin zero particles; the spin-orbit terms of the optical potentials are included as well as the full operator structure of the CD-Bonn potential for the np pair. The calculations include np partial waves with total angular momentum $I \leq 3$, nA partial waves with orbital angular momentum $L \leq 8$, and pA partial waves with $L \leq 20$; the total three-particle angular momentum is $J \leq 35$. Depending on the reaction and energy, some of these quantum numbers cutoffs can be safely chosen significantly lower, leading, nevertheless, to well converged results. The pA channel is more demanding than the nA channel due to the screened Coulomb force, where the screening radius $R \approx 10$ fm for the short-range part of the scattering amplitude is sufficient for convergence. The only exception are reactions leading to a final (Ap) bound state where $R \approx 15$ fm and a sharper screening is needed. With the above choice of the calculational parameters we obtain well converged results for all considered observables such that all discrepancies with the experimental data can be attributed solely to the shortcomings of the interaction models that are used.

3.1 Model 1 - Energy-independent optical potentials

In this case we use the traditional approach based on energy-independent optical potentials whose parameters are chosen at a fixed energy. For deuteron scattering from nucleus A the parameters for the nA and pA potentials are taken from Ref. [6] at half the lab energy of the deuteron projectile. For proton scattering from the (An) nucleus the pA parameters are taken from Ref. [6] at the lab energy of the proton beam and the nA parameters at zero energy, where the imaginary part of the nA optical potential is zero. Small adjustments to these nA parameters are made in order to be able to reproduce the experimental binding energies of the ground and excited single particle states of the

(An) nucleus while all Pauli forbidden bound states of the resulting potential are removed as described in Ref. [20]. Original [6] and adjusted values of these parameters are given in Table 1 for N-^{12}C and N-^{16}O interactions. In the present model only the modified nA parameters are used in given partial waves leading to the single particle states listed in Table 2 for ^{13}C and ^{17}O; in all other nA partial waves we used the original parameters [6] as well as for the pA optical potential. While in $d + A$ scattering the pA and nA potentials are complex, in $p + (An)$ scattering only the pA potential is complex. Although in both cases we are dealing with the same particles, the Hamiltonians are different and, therefore, in $d + A$ we cannot calculate $d + A \rightarrow p + (An)$, but in $p + (An)$ we can calculate the inverse reaction $p + (An) \rightarrow d + A$, or even $p + (An) \rightarrow p + (An)^*$, because the nA interaction is real, in contrast to $d + A$ where it is complex.

Table 1. Original parameters of the real part of the nucleon-nucleus optical potential [6] (first line) and those adjusted to the energies of bound states or resonances in given partial waves, all in units of MeV. The strength of the central part is related to v_R as $V_R = v_R + 0.4ZA^{-1/3} \pm 27.0(N-Z)/A - 0.3E_{\rm c.m.}\Theta(E_{\rm c.m.})$ and V_{so} is the strength of the spin-orbit part; see Ref. [6] for more details.

	$v_R(nA)$	$v_R(pA)$	$V_{so}(nA)$	$V_{so}(pA)$
Ref. [6]	60.00	60.00	5.5	5.5
N-^{12}C (s)	67.50	66.47		
N-^{12}C (p)	61.67	61.50	20.38	20.83
N-^{12}C (d)	66.42	66.42	5.5	5.5
N-^{16}O (s)	61.65	60.94		
N-^{16}O (d)	61.47	60.89	5.4	5.4

Results for these studies are shown by the dotted curves (M1) in Figs. 1–3 for $d + ^{12}$C and $p + ^{13}$C and Figs. 4–6 for $d + ^{16}$O and $p + ^{17}$O at different energies. As mentioned above the results shown by the dotted curves in Fig. 1 (Fig. 4) are obtained with a different Hamiltonian from those in Figs. 2–3 (Figs. 5–6). In general the description of the data for elastic scattering is fairly reasonable and within what can be expected from corresponding CDCC calculations. For the transfer reactions $p + ^{13}\text{C} \rightarrow d + ^{12}\text{C}$ and $p + ^{17}\text{O} \rightarrow d + ^{16}\text{O}$ shown in Fig. 3 and Fig. 6 respectively, one gets a reasonable agreement with data in the forward direction (except for a scaling factor), but deviations from data increase for $\Theta_{\rm c.m.} > 30°$.

The fact that traditional three-body models of $d + A$ and $p + (An)$ scattering are inconsistent with each other encouraged us to study other possibilities in order to shed light on the sensitivity of results to different dynamical approaches.

3.2 Model 2 - Energy-dependent optical potentials

The two-body t-matrix given by Eq. 5 enters the Faddeev/AGS equation 4 for the transition operator $U_{\beta\alpha}(Z)$. Even if the potential is energy independent, the pair t-matrix has to be calculated at the two-body energies $e = E -$

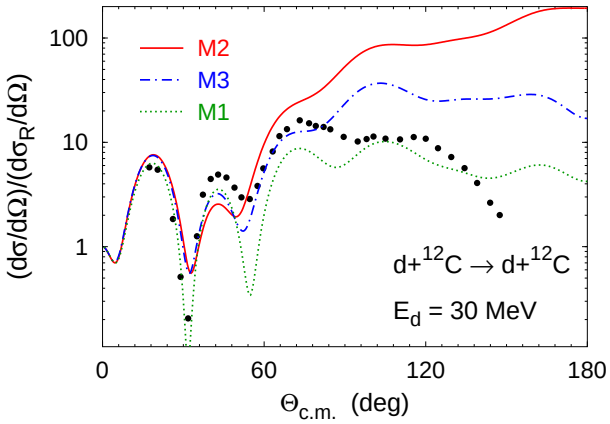

Fig. 1. (Color online) Differential cross section divided by Rutherford cross section for $d + ^{12}$C elastic scattering at $E_d = 30$ MeV. Predictions of Model 1 (dotted curve), Model 2 (solid curve), and Model 3 (dashed-dotted curve) are compared with the experimental data are from Ref. [21].

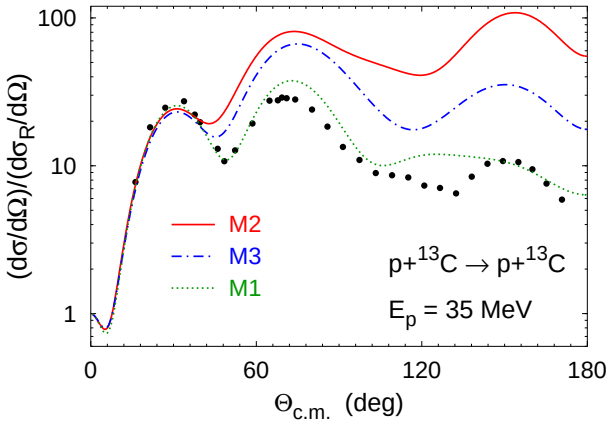

Fig. 2. (Color online) Differential cross section divided by Rutherford cross section for $p + ^{13}$C elastic scattering at $E_p = 35$ MeV. Curves as in Fig. 1. The experimental data are from Ref. [22].

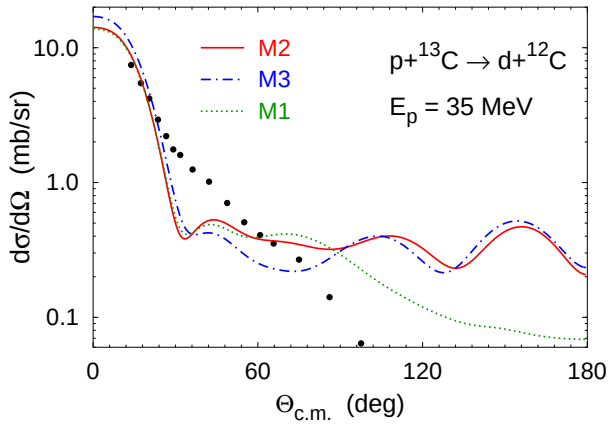

Fig. 3. (Color online) Differential cross section for $p + ^{13}\text{C} \rightarrow d + ^{12}$C transfer at $E_p = 35$ MeV. Curves as in Fig. 1. The experimental data are from Ref. [23].

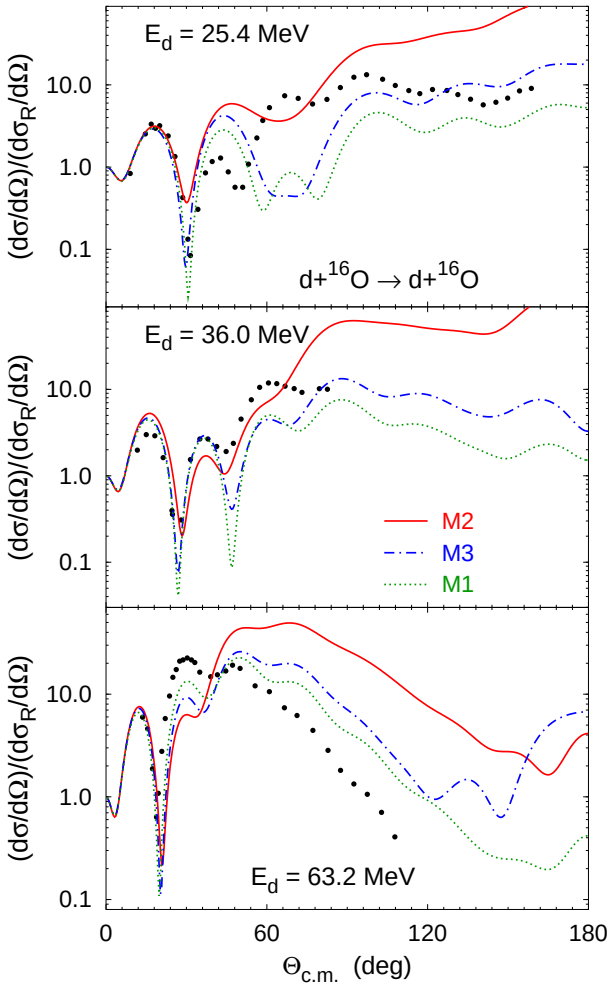

Fig. 4. (Color online) Differential cross section divided by Rutherford cross section for d + ^{16}O elastic scattering at E_d = 25.4, 36.0, and 63.2 MeV. Curves as in Fig. 1. The experimental data are from Refs. [24,25].

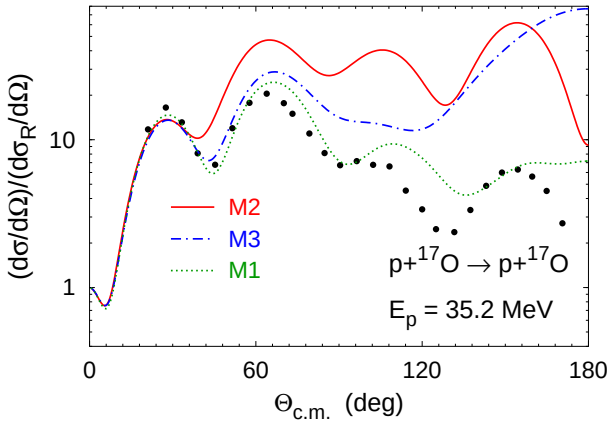

Fig. 5. (Color online) Differential cross section divided by Rutherford cross section for p + ^{17}O elastic scattering at E_p = 35.2 MeV. Curves as in Fig. 1. The experimental data are from Ref. [22].

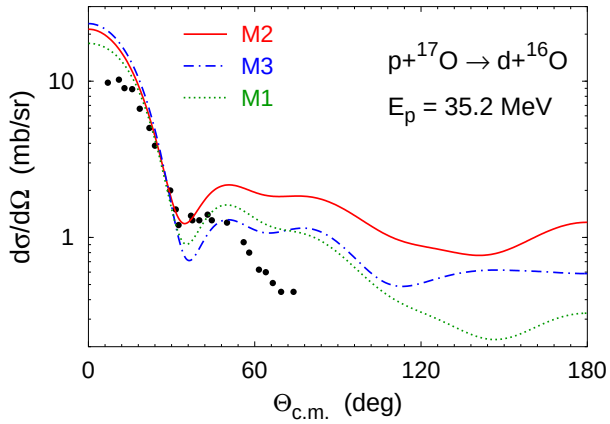

Fig. 6. (Color online) Differential cross section for p + ^{17}O → d + ^{16}O transfer at E_p = 35.2 MeV. Curves as in Fig. 1. The experimental data are from Ref. [24].

$q_\alpha^2/2\mu_\alpha$, where q_α is the relative momentum between particle α and the c.m. of pair α that has to be integrated over when solving the Faddeev/AGS equation, μ_α is the corresponding particle-pair α reduced mass, and E is three-body energy in the c.m. system. Therefore in three-body calculations the particles in all pairs scatter at two-body energies between E and $-\infty$. In the case of the CD-Bonn potential np observables are described with χ^2/datum ~ 1 from zero np relative energy to the π production threshold. The same cannot be said about the nA and pA optical potentials which in the previous model were chosen at a fixed energy. Hence they describe the corresponding data at that energy but not over the broader range that is relevant for the solution of the three-body Faddeev/AGS equation.

In the present model we take the full energy dependence of the optical potential such that when nA or pA pairs interact at a given positive relative energy, the used parameters of the optical potential fit elastic nA and pA scattering at that energy. In addition, when the energy becomes negative the corresponding potentials become real, energy-independent and support a number of bound states that correspond to the ground and excited states of the (An) and (Ap) nucleus whereas the Pauli forbidden states are removed. As mentioned before, the parameters of the energy-dependent optical potentials are slightly modified to obtain the experimental binding energies at zero energy as indicated in Table 1 for both nA or pA potentials in given partial waves. In addition, the binding energy of the Pauli forbidden $1p_{3/2}$ state in ^{13}C and ^{13}N systems is fitted to the ^{12}C neutron and proton separation energy, respectively, whereas the $1p_{1/2}$ binding energy in ^{17}O and ^{17}F systems calculated with original parameters [6] is close to the corresponding nucleon separation energies of ^{16}O. The resulting binding energies are given in Table 2 for ^{13}C, ^{13}N, ^{17}O, and ^{17}F nuclei. In the case of N-^{12}C, where the adjusted parameters are quite different from the original ones, at positive energies v_R is replaced by $v_R(E_{\rm c.m.}) = 60.0 + (v_R - 60.0)\exp(-E_{\rm c.m.}/2)$ and V_{so} is replaced by $V_{so}(E_{\rm c.m.}) = 5.5 + (V_{so} - 5.5)\exp(-E_{\rm c.m.}/2)$, such that the potential preserves the description of the N-^{12}C scattering data in the desired energy regime and remains a continuous

function of the energy. Such a replacement is not needed in the case of N-^{16}O where the adjusted parameters are very close to the original ones.

Using energy-dependent pair interactions in three-body calculations is by no means free of theoretical complications, such as the problem of non-orthogonality of three-body wave functions at different energies as a result of the absence of a Hamiltonian theory for the scattering process. This issue was extensively discussed in Ref. [26] where some of these results were presented first.

Table 2. Binding energies (MeV) of the bound states corresponding to the potential parameters of Table 1. Pauli forbidden bound states that are removed are marked with *.

	$1s_{1/2}$	$2s_{1/2}$	$1p_{3/2}$	$1p_{1/2}$	$1d_{5/2}$
^{11}Be	28.730*	0.503	6.812*	0.183	
^{13}C	38.022*	1.857	18.722*	4.946	1.092
^{13}N	33.864*		15.957*	1.944	
^{17}O	37.213*	3.272	19.267*	16.067*	4.143
^{17}F	32.559*	0.105	15.561*	12.348*	0.600

In Fig. 1–11 the solid curves (M2) show the results of the present fully energy-dependent model for all possible reactions at different energies. A number of interesting features emerge:

a) Elastic scattering results shown in Figs. 1, 2, 4, and 5 differ quite strongly from Model 1 (dotted curves), particularly at large angles, and become considerably worse when compared to data.
b) In the low angular region ($\Theta_{\rm c.m.} < 30°$) $p + {}^{13}\mathrm{C} \to d + {}^{12}\mathrm{C}$ (Fig. 3) and $p + {}^{17}\mathrm{O} \to d + {}^{16}\mathrm{O}$ (Fig. 6) results are very similar to those obtained with Model 1 except for a small scaling factor.
c) Fig. 7 shows new results for the transfer reactions $d + {}^{12}\mathrm{C} \to p + {}^{13}\mathrm{C}$ to ground state $1/2^-$ and excited states $1/2^+$ and $5/2^+$. Again up to $\Theta_{\rm c.m.} \simeq 30°$ the calculation follows the data within a small scaling coefficient that may be associated with a spectroscopic factor. In the case of the transfer to the ground state, solid curves in Figs. 3 and 7 have similar shape as expected by detailed balance taking into account the small difference in the energies. The calculations also reflect the qualitative features of the data.
d) Figs. 9 and 10 show new results for the transfer reactions $d + {}^{16}\mathrm{O} \to p + {}^{17}\mathrm{O}$ to ground state $5/2^+$ and excited state $1/2^+$. Again the calculations describe the qualitative features of the data though scaling factors may be needed.
e) Figs. 8 and 11 show new results for $p + {}^{13}\mathrm{C} \to n + {}^{13}\mathrm{N}$ ground state $1/2^-$ and $p + {}^{17}\mathrm{O} \to n + {}^{17}\mathrm{F}$ ground state $5/2^+$ and excited state $1/2^+$. Although in the charge exchange reactions to the ground state the data is not described successfully, it is worth noting that in $p + {}^{17}\mathrm{O} \to n + {}^{17}\mathrm{F}$ excited state $(1/2^+)$ the calculations are in very reasonable agreement with data, except for a small scaling factor.

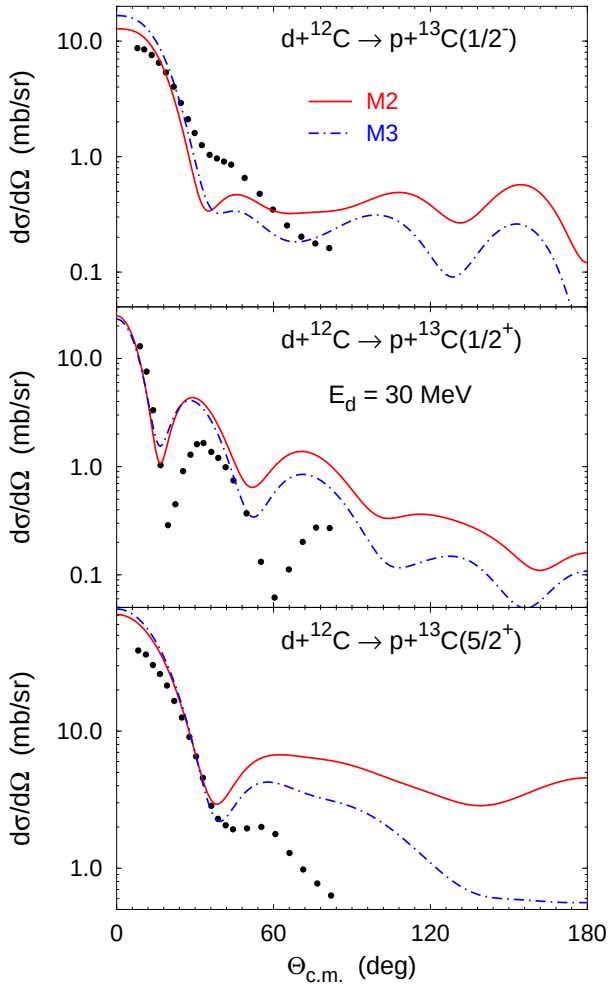

Fig. 7. (Color online) Differential cross section for $d + {}^{12}\mathrm{C} \to p + {}^{13}\mathrm{C}$ transfer at $E_d = 30$ MeV. Predictions of Model 2 (solid curve) and Model 3 (dashed-dotted curve) are compared with the experimental data from Ref. [27].

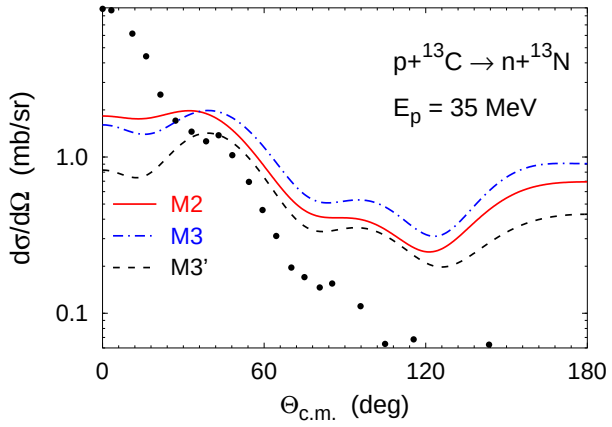

Fig. 8. (Color online) Differential cross section for $p + {}^{13}\mathrm{C} \to n + {}^{13}\mathrm{N}$ reaction at $E_p = 35$ MeV. Dashed curve is the prediction of Model 3', other curves as in Fig. 7. The experimental data are from Ref. [28].

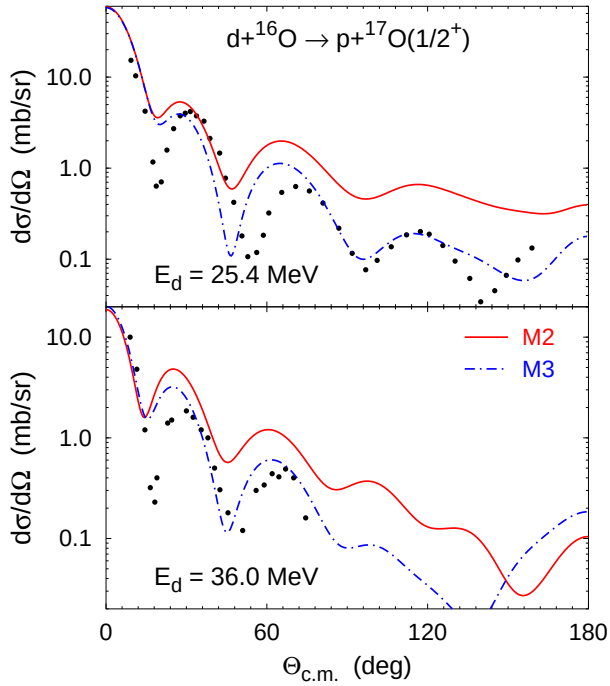

Fig. 9. (Color online) Differential cross section for $d + {}^{16}\mathrm{O} \rightarrow p + {}^{17}\mathrm{O}$ transfer at $E_d = 25.4$ and 36.0 MeV. Curves as in Fig. 7. The experimental data are from Ref. [24].

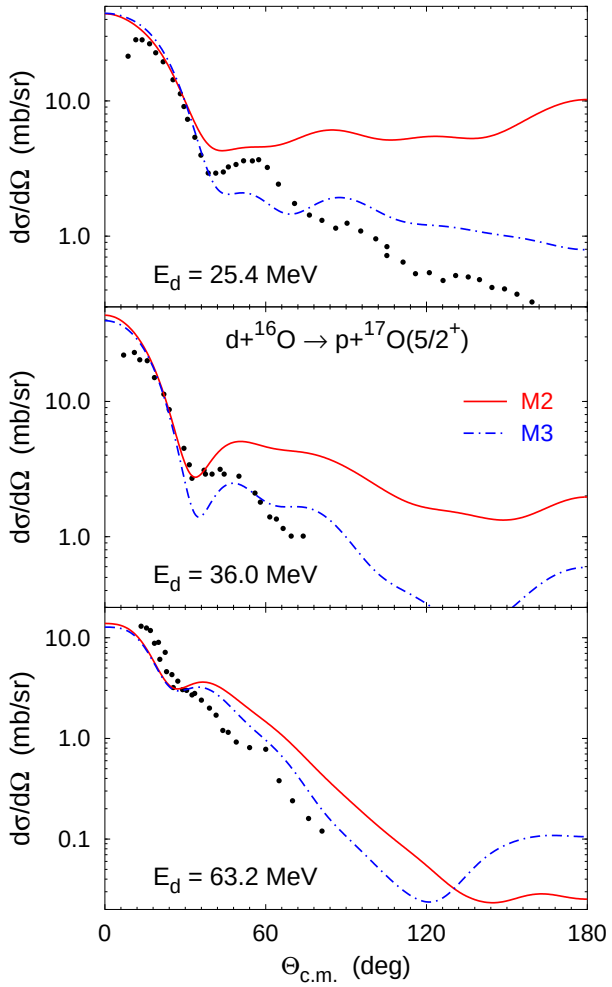

Fig. 10. (Color online) Differential cross section for $d + {}^{16}\mathrm{O} \rightarrow p + {}^{17}\mathrm{O}$ transfer at $E_d = 25.4$, 36.0, and 63.2 MeV. Curves as in Fig. 7. The experimental data are from Ref. [24].

It is worth noting at this point that a good description of elastic data beyond small angles does not seem to be necessary to get the right magnitude of the transfer cross sections at small angles since Figs. 3 and 6 show similar results for two distinct models that lead to very different results for the elastic cross sections at large angles (see Figs. 1, 2, 4, 5).

3.3 Model 3 - A "hybrid" optical potential approach

Having studied these two extreme dynamical model approaches, the energy-independent and the fully energy-dependent, we attempt to study a combination of the two. Since we want that the relevant nuclei, ^{13}C, ^{13}N, ^{17}O, and ^{17}F have the proper low-energy spectra in order to describe all the relevant transfer reactions discussed before, we use in this case a partial-wave dependent optical potential in the following way: *a)* For $d + A$ reactions in N-^{12}C (N-^{16}O) s, p, and d waves (s and d waves) we use the energy-dependent optical potentials of Model 2; for $p + (An)$ reactions the pA potential in the above mentioned partial waves is energy-dependent as well, but the nA potential is taken over from Model 1 since it is sufficient to bind ^{13}C and ^{17}O; *b)* In all other partial waves we use the energy-independent optical potentials of Model 1 with a few nuances that are explained in the text, depending on whether we have $d + A$ or $p + (An)$ scattering.

Since Model 1 is more absorptive than Model 2 due to the large impact of the imaginary part of the optical interactions on the elastic cross sections we expect this hybrid model to improve the description of the elastic data.

For $d + A$ scattering, results are shown by the dash-dotted curves (M3) in Figs. 1, 4, 7, 9, and and 10. In $d + {}^{12}\mathrm{C}$ ($d + {}^{16}\mathrm{O}$) both nA and pA optical potentials are, like in Model 2, energy dependent in s, p, and d waves (s and d waves) while in all other partial waves they are energy independent with the parameters chosen at half the deuteron lab energy like in Model 1. The dash-dotted curves show a remarkable improvement vis-à-vis the fully energy-dependent calculations (solid lines in Model 2), particularly at large angles. This effect is visible not only in elastic scattering (Figs. 1 and 4), but also in the transfer reactions $d + A \rightarrow p + (An)$ shown in Figs. 7, 9, and 10 where in some specific cases such as in Figs. 9 and 10 one gets quite reasonable description of the data.

For p+(An) scattering results are again shown in Figs. 2, 3, 5, 6, 8, and 11 by the dash-dotted curves (M3). In $p + {}^{13}\mathrm{C}$ ($p + {}^{17}\mathrm{O}$) the pA optical potentials are, like in Model 2, energy dependent in s, p, and d waves (s and d waves) and, in all other partial waves, are energy independent with the parameters chosen at the proton lab energy, like in Model 1. As for the nA optical potential it is chosen as in Model 1 where, in all partial waves the potential is real and sup-

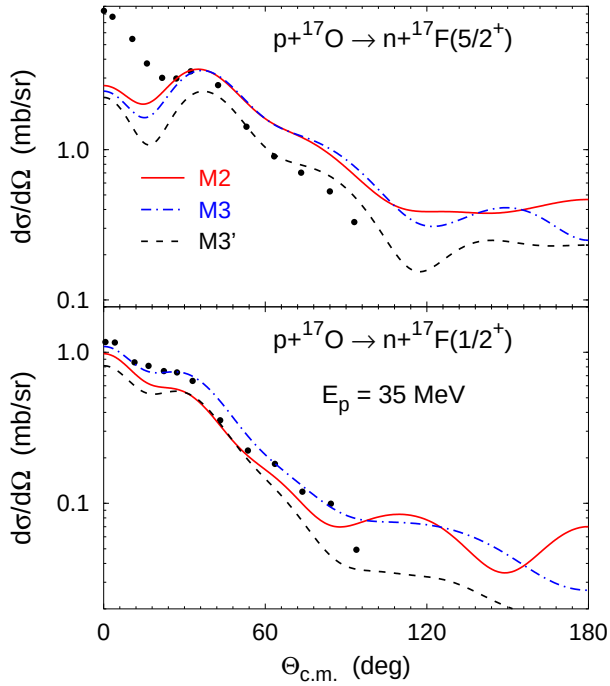

Fig. 11. (Color online) Differential cross section for $p + {}^{17}\mathrm{O} \rightarrow n + {}^{17}\mathrm{F}$ reaction at $E_p = 35$ MeV. Curves as in Fig. 8. The experimental data are from Ref. [29].

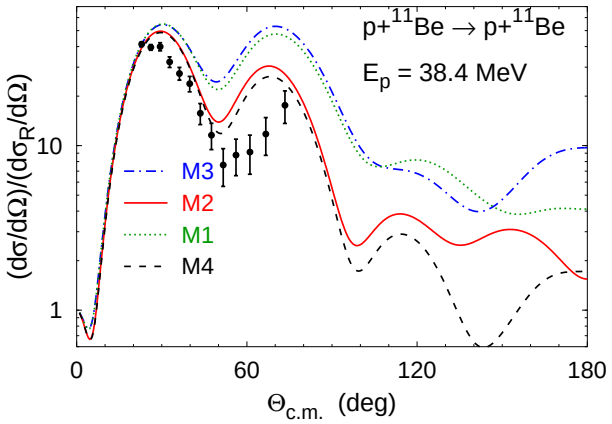

Fig. 12. (Color online) Differential cross section divided by Rutherford cross section for $p + {}^{11}\mathrm{Be}$ elastic scattering at $E_p = 38.4$ MeV. Curves as in Fig. 1 plus predictions of the Model 4 as described in the text. The experimental data are from Ref. [34].

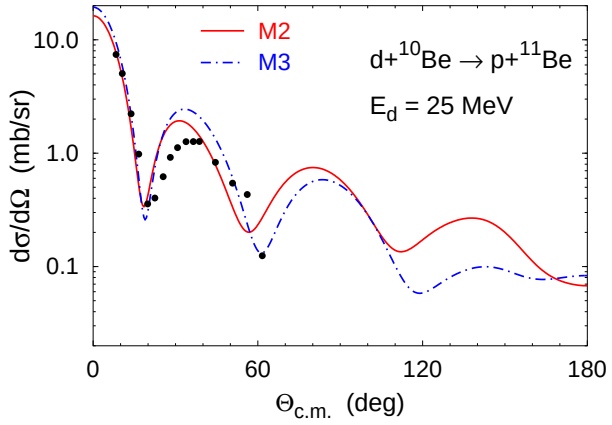

Fig. 13. (Color online) Differential cross section for $d + {}^{10}\mathrm{Be} \rightarrow p + {}^{11}\mathrm{Be}$ transfer at $E_d = 25$ MeV. Curves as in Fig. 1. The experimental data are from Ref. [35].

ports a number of single particle states as mentioned before. As in $d + A$ reactions, we notice an improvement in the description of $p + (An)$ elastic (Figs. 2 and 5) as well as $p + (An) \rightarrow d + A$ transfer (Figs. 3 and 6) observables. Nevertheless, at small angles ($\Theta_{\mathrm{c.m.}} \leq 30°$), the differences between Models 1, 2, and 3 are quite small indicating that the extracted spectroscopic factors would be of similar size as well.

Finally for the charge transfer reactions shown in Figs. 8 and 11 we add a new calculation shown by the dashed curves (M3') where the nA optical potential is energy-dependent in the s, p, and d partial waves for ${}^{13}\mathrm{C}$ and s and d waves for ${}^{17}\mathrm{O}$ like in Model 2 but is, in the other partial waves, energy-independent with the parameters chosen according to the lab energy of the neutron in the inverse reaction $n + (Ap) \rightarrow p + (An)$. The three curves shown in Figs. 8 and 11 are not very different aside a scaling factor.

3.4 Reactions involving one-neutron halo nucleus ^{11}Be

In Figs. 12 and 13 we present results for $p + {}^{11}\mathrm{Be}$ elastic scattering and $d + {}^{10}\mathrm{Be} \rightarrow p + {}^{11}\mathrm{Be}$ transfer reaction. In these calculations the $n - {}^{10}\mathrm{Be}$ interaction used in Model 1 and Model 3 for $p + {}^{11}\mathrm{Be}$ elastic scattering is taken from Ref. [33] leading to the bound states for ${}^{11}\mathrm{Be}$ shown in Table 2; in Model 2 we use the parameters of Ref. [33] when the pair kinetic energy is negative and those of Ref. [6] when it is positive. The prescription described in Subsec. 3.2 is used to make the potential a continuous function of the energy. The corresponding $p - {}^{10}\mathrm{Be}$ interaction used in Models 1, 2, and 3 is from Ref. [6]. Likewise, in $d + {}^{10}\mathrm{Be}$ we use in Models 2 and 3 the same potentials as in $p + {}^{11}\mathrm{Be}$.

For this particular reaction we find that the effect of the optical potential energy dependence is very different compared to $p + {}^{13}\mathrm{C}$ or $p + {}^{17}\mathrm{O}$ elastic scattering. The energy dependence in the pA optical potential plays only a minor role, except for backward angles, whereas the energy dependence in the nA optical potential yields additional absorption that strongly reduces the elastic cross section for $\Theta_{\mathrm{c.m.}} > 30°$. To illustrate this we show the predictions of Model 4 where the pA optical potential is energy independent as in Model 1 but the nA optical potential is energy dependent as in Model 2.

4 Conclusions

We have used the Faddeev/AGS three-body approach to study $d + {}^{10}\mathrm{Be}$, $d + {}^{12}\mathrm{C}$, $d + {}^{16}\mathrm{O}$, $p + {}^{11}\mathrm{Be}$, $p + {}^{13}\mathrm{C}$, and

$p+{}^{17}$O reactions as a three-body system made up by a proton p, a neutron n and a structureless nuclear core A, the ^{10}Be, ^{12}C or ^{16}O. The interactions between pairs are the realistic interactions that describe np, nA, and pA scattering over the relevant energy range. The Coulomb interaction between the proton and the nuclear core is included in a numerically exact (converged) way.

The aim of the present work is to demonstrate the possibilities and the shortcomings of the Faddeev/AGS three-body approach that provides, simultaneously, predictions for all possible reactions, i.e., elastic, transfer and charge exchange such as, for example, $p + {}^{17}\mathrm{O} \rightarrow p + {}^{17}\mathrm{O}$, $p + {}^{17}\mathrm{O} \rightarrow d + {}^{16}\mathrm{O}$, and $p + {}^{17}\mathrm{O} \rightarrow n + {}^{17}\mathrm{F}$, or $d + {}^{16}\mathrm{O} \rightarrow d + {}^{16}\mathrm{O}$, $d + {}^{16}\mathrm{O} \rightarrow p + {}^{17}\mathrm{O}$, and $d + {}^{16}\mathrm{O} \rightarrow n + {}^{17}\mathrm{F}$, as well as $p + {}^{11}\mathrm{Be} \rightarrow p + {}^{11}\mathrm{Be}$ and $d + {}^{10}\mathrm{Be} \rightarrow p + {}^{11}\mathrm{Be}$.

Three different models (M1, M2, M3) are studied involving energy-independent and energy-dependent optical potentials that fit the nA and pA elastic scattering and whose parameters are fixed at a chosen energy or are allowed to vary over the energy range of the interacting pair, respectively. In the case of energy-dependent optical potentials these become real at negative energies and support a number of single particle states that characterize the (An) or the (Ap) nucleus.

The results of our calculations indicate that transfer and charge exchange reactions at small angles are rather insensitive to the chosen model, but the elastic scattering cross sections are highly sensitive to the choice of energy dependence of the optical interaction (M1 versus M2 and M3). Comparison with published CDCC, DWBA, CCBA, and adiabatic calculations indicates that these approximate methods provide, in general, a better fit of the data than our calculations but are qualitatively similar to our results, particularly the ones of the "hybrid" model M3 that uses a partial-wave dependent optical potential whose parameters are energy-independent except in the partial waves that support the single particle states of the (An) and (Ap) nuclei.

References

1. N. Austern, Y. Iseri, M. Kamimura, M. Kawai, G. Rawitscher, and M. Yahiro, Phys. Rep. **154**, (1987) 125.
2. S. T. Butler, *Proc. Roy. Soc. (London)* **A208**, (1951) 559.
3. L. D. Faddeev, Zh. Eksp. Teor. Fiz. **39**, (1960) 1459 [Sov. Phys. JETP **12**, (1961) 1014].
4. E. O. Alt, P. Grassberger, and W. Sandhas, Nucl. Phys. **B2**, (1967) 167.
5. W. Glöckle, *The Quantum Mechanical Few-Body Problem* (Springer-Verlag, Berlin/Heidelberg, 1983).
6. B. A. Watson, P. P. Singh, and R. E. Segel, Phys. Rev. **182**, (1969) 978.
7. R. Machleidt, Phys. Rev. C **63**, (2001) 024001.
8. R. Aaron and P. E. Shanley, Phys. Rev. **142**, (1966).
9. E. O. Alt, L. D. Blokhintsev, A. M. Mukhamedzhanov, and A. I. Sattarov, Phys. Rev. C **75**, (2007) 054003.
10. A. Deltuva, A. C. Fonseca, and P. U. Sauer, Phys. Rev. C **71**, (2005) 054005; **72**, (2005) 054004; **73**, (2006) 057001.
11. A. Deltuva, A. C. Fonseca, and P. U. Sauer, Phys. Rev. Lett. **95**, (2005) 092301.
12. J. R. Taylor, Nuovo Cimento **B23**, (1974) 313 ; M. D. Semon and J. R. Taylor, *ibid.* **A26**, (1975) 48.
13. E. O. Alt, W. Sandhas, and H. Ziegelmann, Phys. Rev. C **17**, (1978) 1981; E. O. Alt and W. Sandhas, *ibid.* **21**, (1980) 1733.
14. A. Deltuva, A. M. Moro, E. Cravo, F. M. Nunes, and A. C. Fonseca, Phys. Rev. C **76**, (2007) 064602.
15. R. Crespo, E. Cravo, A. Deltuva, M. Rodríguez-Gallardo, and A. C. Fonseca, Phys. Rev. C **76**, (2007) 014620.
16. R. Crespo, A. Deltuva, E. Cravo, M. Rodríguez-Gallardo, and A. C. Fonseca, Phys. Rev. C **77**, (2008) 024601.
17. K. Chmielewski, A. Deltuva, A. C. Fonseca, S. Nemoto, and P. U. Sauer, Phys. Rev. C **67**, (2003) 014002.
18. A. Deltuva, K. Chmielewski, and P. U. Sauer, Phys. Rev. C **67**, (2003) 034001.
19. A. Deltuva, A. C. Fonseca, and P. U. Sauer, Annu. Rev. Nucl. Sci. **58**, (2008) 27.
20. A. Deltuva, Phys. Rev. C **74**, (2006) 064001.
21. G. Perrin, Nguyen Van Sen, J. Arvieux, R. Darves-Blanc, J. L. Durand, A. Fiore, J. C. Gondrand, F. Merchez, and C. Perrin, Nucl. Phys. **A282**, (1977) 221.
22. E. Fabrici, S. Micheletti, M. Pignanelli, F. G. Resmini, R. De Leo, G. D'Erasmo, and A. Pantaleo, Phys. Rev. C **21**, (1980) 844.
23. H. Toyokawa, H. Ohnuma, Y. Tajima, T. Niizeki, Y. Honjo, S. Tomita, K. Ohkushi, M. H. Tanaka, S. Kubono, M. Yosoi, Phys. Rev. C **51**, (1995) 2592.
24. M. D. Cooper, W. F. Hornyak, and P. G. Roos, Nucl. Phys. **A218**, (1974) 249.
25. E. Newman, L. C. Becker, B. M. Preedom, and J. C. Hiebert, Nucl. Phys. **A100**, (1967) 225.
26. A. Deltuva and A. C. Fonseca, Phys. Rev. C **79**, (2009) 014606.
27. H. Ohnuma *et al.*, Nucl. Phys. **A448**, (1986) 205.
28. H. Ohnuma *et al.*, Nucl. Phys. **A456**, (1986) 61.
29. M. Oura *et al.*, Nucl. Phys. **A586**, (1995) 20.
30. R. C. Johnson and P. J. R. Soper, Phys. Rev. C **1**, (1970) 976.
31. R. C. Johnson, J. S. Al-Khalili, and J. A. Tostevin, Phys. Rev. Lett. **79**, (1997) 2771.
32. N. K. Timofeyuk and R.C. Johnson, Phys. Rev. C **59**, (1999) 1545.
33. R. Crespo, E. Cravo, A. Deltuva, M. Rodríguez-Gallardo and A. C. Fonseca, Phys. Rev. C **76**, (2007) 014620.
34. V. Lapoux *et al.*, Phys. Lett. **B658**, (2007) 198.
35. B. Zwieglinski, W. Benenson, R. Robertson, and W. Coker, Nucl. Phys. **A315**, (1979) 124.